Chinese Journal of
POLYMER SCIENCE

ARTICLE

https://doi.org/10.1007/s10118-019-2178-3
Chinese J. Polym. Sci. **2019**, *37*, 164–177

Modeling of the Mechanical Properties of Blend Based Polymer Nanocomposites Considering the Effects of Janus Nanoparticles on Polymer/Polymer Interface

Esmail Sharifzadeh*

Department of Chemistry, Payame Noor University, Tehran, Iran

Electronic Supplementary Information

Abstract Blend based polymer nanocomposites, comprising Janus nanoparticles at their polymer/polymer interface, were analytically/experimentally evaluated. The modeling procedure was performed in two stages: first, modeling of polymer/polymer interface region comprising Janus nanoparticles and second, modeling of the entire systems as a function of the variation of the blend morphology. In the first stage, the modeling procedure was performed based on the development of the model proposed by Ji *et al*. and in the second stage, the fundamental of Kolarik's model was used in order to propose a developed and more practical model. It was shown that Janus nanoparticles may form dual polymer/particle interphase at polymer/polymer interface which can drastically affect the final mechanical properties of the system. Comparing the results of tensile tests imposed on different prepared samples with the predictions of the model proved its accuracy and reliability (error < 9%).

Keywords Blend based polymer nanocomposites; Janus nanoparticles; Modeling of mechanical properties

Citation: Sharifzadeh, E. Modeling of the mechanical properties of blend based polymer nanocomposites considering the effects of Janus nanoparticles on polymer/polymer Interface. *Chinese J. Polym. Sci.* **2019**, *37*, 164–177.

INTRODUCTION

Enhancing the mechanical or physical properties of a polymer material has always been considered as a very important and interesting aspect of investigation.[1] Applying nanoparticles or other polymers to a polymer base is one of the well-known methods to manipulate its properties.[2–12] Considering many parameters associated with the enhancement of mechanical/physical properties of a polymer base in a nanocomposite (*e.g.* the type and shape of nanoparticle, filler/polymer interaction, adequate dispersion/distribution of nanoparticles, *etc*.) or a polymer blend (*e.g.* polymer/polymer interaction, content of the dispersed phase, *etc*.), precise control of its final properties is quite challenging.[5,6,11,13,14] Nevertheless, it is proved that the simultaneous application of these two methods is a very practical approach to design the final desirable mechanical or physical properties of a polymer base.[15,16] In such blend-based nanocomposites (BBNs), besides the blend morphology, the placement site of nanoparticles (in major/minor phase or at the polymer/polymer interface of immiscible polymer) significantly affects their reinforcing performance.[17,18] The spontaneous migration of common nanofillers (*e.g.* CNT, silica, clay) toward polymer/polymer interface in a BBN system requires specific arrangement (such as specific surface chemical modification), which limits the production of such systems.[15,19,20]

Janus nanoparticles are a special type of nanoparticles whose surface has two or more distinct chemical properties that make them more compatible with the phase interface (of specific systems) compared to common nanoparticles.[20–26] Recently, there have been significant advances in preparing such nanomaterials as monodispersed nano-objects, and it is now the matter of tailoring their properties *via* surface modification,[27,28] which has led to nanoparticles with isotropic surficial chemistry.[29] Accordingly, these special nanoparticles are the best choice for producing BBN systems comprising nanoparticles at their polymer/polymer interface.

On the other hand, applying analytical models has always been considered as a reliable method to predict the characteristics of different systems such as polymer nanocomposites and blends.[30–37] Nevertheless, the number of such models that are capable of predicting the final mechanical or physical properties of a BBN is not significant, which can be attributed to the complexity caused by the abundance of effective parameters such as the effects of polymer/particle interphase, polymer/polymer interface, blend morphology and random orientation of nanoparticles on the final properties.[38–42] In our previous work, considering the placement of nanoparticles in major/minor phase, knotted approximation (KA) model was proposed for predicting the tensile modulus of

* Corresponding author: E-mail E_sharifzadeh@sut.ac.ir

Received June 23, 2018; Accepted August 1, 2018; Published online August 31, 2018

BBNs.[38] KA model had a three-step procedure: first, to predict the tensile modulus of the nanoparticle-containing phase using numerical approximation system (NAS) model (a developed form of the model proposed by Ji *et al*.[43]);[31] second, to consider the BBN system as a simple polymer blend comprising a polymer phase (minor/major) and the nanoparticle-containing phase; and the final step, to predict the tensile modulus of the final polymer blend using direct and independent approximation model (DIA)[30] (combination of Maxwell-Eucken[44] and Kolarik model[45]) or symmetrical approximation system (SAS)[32] (developed form of KISS model proposed by Wang *et al*.[44]). However, it should be mentioned that KA model is not applicable in the case of BBN systems comprising nanoparticles at polymer/polymer interface while it provides acceptably accurate predictions in other cases. A comprehensive description of KA model is represented in the electronic supplementary information (ESI, section S1).

Accordingly, in this work, a developed form of KA model is proposed to predict the tensile modulus of a BBN system comprising Janus nanoparticles at their polymer/polymer interface which is referred to as KAd. Generally, KAd applies the fundamentals of the models proposed by Kolarik *et al*., Maxwell-Eucken and also Wang *et al*. As mentioned before, the placement of common nanoparticles at the polymer/polymer interface in a BBN system is quite challenging and this definitely makes Janus nanoparticles as a perfect choice for such systems. Accordingly, a combination of methods proposed in our previous works was used in order to prepare spherical silica Janus nanoparticles which were proved to be capable of migrating toward PS/PMMA interface.[20,46] In another work, an analytical/experimental method was proposed in order to investigate the adsorption of different-sized spherical silica particles at the oil/water interface in a Pickering emulsion system.[47] This method could help us to simulate the surface chemical structure of the produced Janus nanoparticles (three-phase contact angle), which is a key parameter to characterize the polymer/nanoparticle interphase of the nanoparticles placed at the polymer/polymer interface in a BBN system.

Moreover, KAd was expanded to cover all possible polymer/nanoparticle interphase structures as well as blend morphology in a BBN system. In order to compare the results of KAd with experimental data, many samples including PS/PMMA/Janus BBN with different contents of Janus nanoparticles, PA/PMMA/Janus BBN with different contents of PMMA and neat PS/PMMA blend with different contents of PMMA were prepared and subjected to tensile test (all samples were prepared *via* solution mixing). The surface chemical structure of the produced Janus nanoparticles was simulated using the mentioned method and the resultant three-phase contact angle was directly used in KAd. All BBN, PS/PMMA and nanocomposite samples were produced *via* solution mixing. It was found that KAd was completely capable of providing reliable results in the case of BBN samples comprising low contents of Janus nanoparticle (error < 7%) while the polymer phase content variation (PS or PMMA) did not significantly affect its performance.

MODELING

Modeling of Polymer/Polymer Interface Region

Generally, the production of Janus nanoparticles *via* desymmetrization process involves the migration of primary hydrophilic (or hydrophobic) nanoparticles toward oil/water interface in Pickering emulsion.[25,46] Reducing the system temperature, after stabilization of the Pickering emulsion (containing melted paraffin as the oil phase), makes the migrated nanoparticles trapped at the oil/water interface (Fig. 1a). Therefore, the buried surface of nanoparticles is completely unavailable in the first surface modification process, while after dissolving the solidified paraffin droplets it is possible

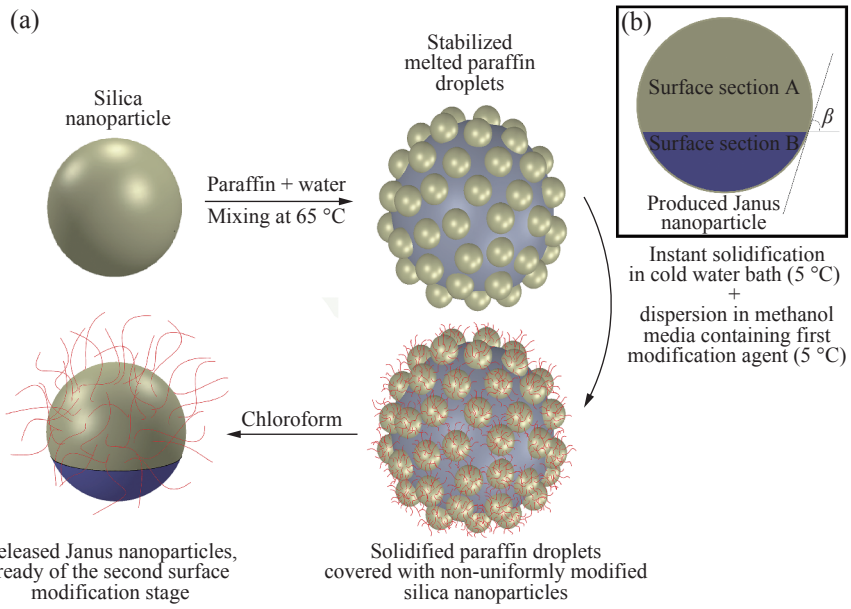

Fig. 1 Schematic of synthesizing process of Janus nanoparticles using Pickering emulsions: (a) migration of hydrophilic silica nanoparticles toward oil/water interface and their primary modification stage[46]; (b) parameter β which defines the share of surface sections A and B

https://doi.org/10.1007/s10118-019-2178-3

to apply second surface modification process on the intact buried surface.[46] The product of this process is Janus nanoparticles with dissymmetrical surface chemistry on which the share of each surface section can be determined using three-phase contact angle (β) (Fig. 1b).

In our previous work, we proposed a method for predicting β using surface and interfacial tension parameters:[47]

$$\cos\beta = \frac{\gamma(\mathrm{WA})\cos\lambda - \gamma(\mathrm{OA})\cos\alpha}{\gamma(\mathrm{OW})} \quad (1)$$

where γ(WA) and γ(OA) are the surface tension of water and oil, respectively, γ(OW) denotes the oil/water interfacial tension, λ and α are the contact angles of water and oil droplets on a silica coated-surface, respectively.

Considering a polymer blend of two phases (I and II) and the presence of their corresponding chemical agents tailored to either surface section of a spherical Janus nanoparticle, it is possible to simulate Janus nanoparticles at the phase (I)/phase (II) interface using parameter β (Fig. 2a). As a result, a BBN system can be assumed as a structure consisting of two polymer phases plus one interface region (Fig. 2b).

Modeling the mechanical properties of the interface region requires careful consideration of some parameters such as the difference between the thickness of polymer/nanoparticle interphases in phase (I) and phase (II), the effects of polymer/nanoparticle interphase on the arrangement of equivalent box models (EBM), the closest possible geometrical similarity between the model structure and the actual base, determination of model parameters based on actual value, *etc*. To this end, we used the fundamentals of the model proposed by Ji *et al*. in order to model the mechanical properties of the polymer/polymer interface region. The hypothetical structure of the model is represented in Fig. 3.

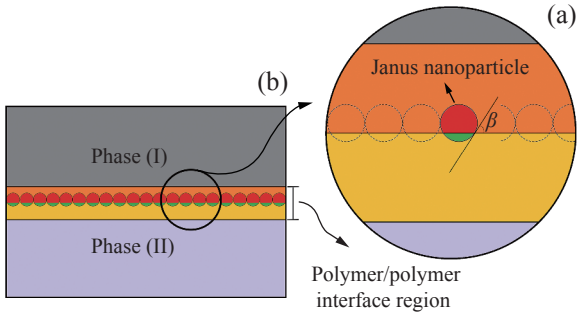

Fig. 2 (a) Penetration depth of Janus nanoparticles in phase (I)/phase (II) interface as a function of parameter β; (b) Schematic of polymer/polymer interface region (Yellow and orange sections represent involved parts of phases (I) and (II) in polymer/polymer interface region, respectively.)

As clearly shown, this geometrical structure implies that the polymer/particle interphase in phase (II) is thicker than the polymer/particle interphase in phase (I) ($k_2 > k_1$) and the whole structure is encircled with a sphere of unit radius. Also, it is assumed that the whole polymer/polymer interface is covered with a monolayer of Janus nanoparticles (not aggregated) (Fig. 2). It should be mentioned that the presented model is a developed form of NAS model and therefore it applies the fundamentals of the model proposed by Ji *et al*.[43] Fig. 3(a) illustrates EBM model corresponding to the assumed geometrical structure. Each EBM box represents an element of the geometrical structure (Fig. 3c) and also has a numerical value equal to the volume fraction of its corresponding element. As shown in Fig. 4, the thickness of polymer/nanoparticle interphases ($k_j - z$) is a function of $\beta'_j|_{j=1,2}$, which makes it possible to correlate them using parameter β:

$$\beta'_j|_{j=1,2} = \arccos\left(\frac{z}{k_j}\cos\beta\right)_{j=1,2} \quad (2a)$$

$$\beta'' = \arccos(z\cos\beta) \quad (2b)$$

where k_j and z are model parameters (Fig. 4).

As a result, the volume of EBM boxes located in part (I) can be calculated as follows:

$$V_{\mathrm{N_{II}}} = \frac{\pi(z(1-\cos\beta))^2}{3}(3z - z(1-\cos\beta)) \quad (3)$$

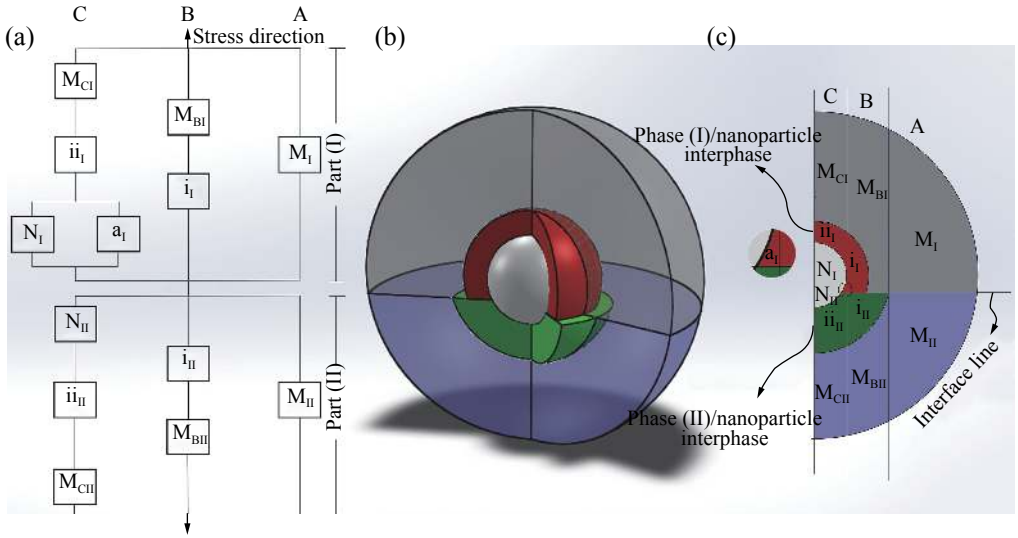

Fig. 3 (a) Equivalent box model (EBM) corresponding to the governing geometrical structure; (b) Hypothetical geometrical structure corresponding to phase (I)/phase (II) interface region (the whole structure is surrounded by a sphere of unit radius), and (c) model components

https://doi.org/10.1007/s10118-019-2178-3

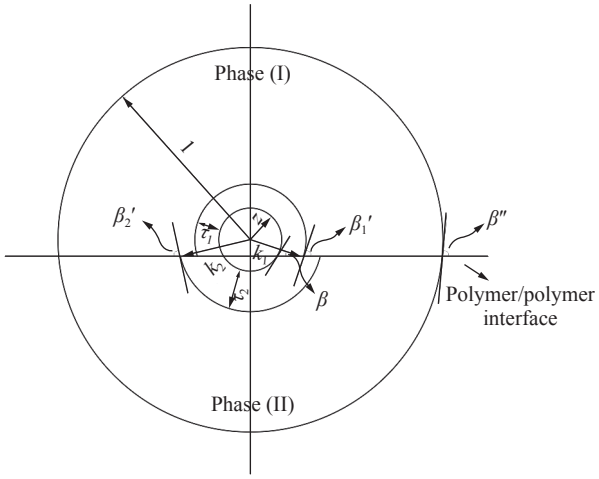

Fig. 4 Schematic of correlation between parameters k_j and β_j. Parameter $\tau_j = k_j - z$ indicates the thickness of polymer/particle interphase.

$$V_{N_I} = \frac{4}{3}\pi z^3 - V_{N_{II}} \tag{4}$$

$$V^{P1}_{i_{II}+i_{II}} = \frac{\pi(k_1(1-\cos\beta'))^2}{3}(3k_1 - (k_1(1-\cos\beta'))) - V_{N_{II}},\ \beta' = f(k_1) \tag{5}$$

$$V^{P1}_{i_{II}} = \frac{\pi(k_1(1-\cos\beta'))^2}{3}(3k_1 - (k_1(1-\cos\beta'))) - (V_{R.T.} + V_{Co.} + V_{S.C.}),\ \beta' = f(k_1) \tag{6a}$$

$$V_{R.T.} = \pi\left(\frac{2}{3}z^2 h\right) \tag{6b}$$

$$V_{Co.} = \frac{\pi z^2 h}{3} \tag{6c}$$

$$V_{S.C.} = \frac{\pi\left(k_1\left[1-\sin\left(\arccos\left(\frac{z}{k_1}\right)\right)\right]\right)^2}{3} \cdot \left(3k_1 - \left(k_1\left[1-\sin\left(\arccos\left(\frac{z}{k_1}\right)\right)\right]\right)\right) \tag{6d}$$

$$h = k_1\left(\sin\left(\arccos\left(\frac{z}{k_1}\right)\right) - \cos\beta'\right),\ \beta' = f(k_1) \tag{6e}$$

$$V^{P1}_{i_{II}} = V^{P1}_{i_{II}+i_{II}} - V^{P1}_{i_{II}} \tag{7}$$

$$V_{i_I} = \frac{4\pi}{3}\left({k_1}^2 - z^2\right)^{\frac{3}{2}} - V^{P1}_{i_{II}} \tag{8}$$

$$V_{ii_I} = \frac{2\pi\left(\left({k_1}^3\right) - \left(\left({k_1}^2 - z^2\right)^{\frac{3}{2}} + z^3\right)\right)}{3} \tag{9}$$

$$V_{a_I} = V_{ii_I} - V^{P1}_{ii_{II}} \tag{10}$$

$$V^{P1}_{M_{II}} = \frac{\pi(1-\cos\beta'')^2}{3}(2+\cos\beta'') - (V_{R.T.} + V_{Co.} + V_{S.C.}) \tag{11a}$$

$$V_{R.T.} = \pi\left(\frac{2}{3}{k_1}^2 h\right) \tag{11b}$$

$$V_{Co.} = \frac{\pi {k_1}^2 h}{3} \tag{11c}$$

$$V_{S.C.} = \frac{\pi(1-\sin(\operatorname{acos} k_1))^2}{3}(2+\sin(\operatorname{acos} k_1)) \tag{11d}$$

$$h = \sin(\operatorname{acos} k_1) - \cos\beta'' \tag{11e}$$

$$V_{M_{CI}} = V^{P1}_{M_{CII}} = \frac{4\pi - 3\left(\frac{4}{3}\pi\left(1-z^2\right)^{\frac{3}{2}} + V_{N_I} + V_{N_{II}} + V_{ii_I} + V^{P1}_{ii_{II}} + V_{a_I}\right)}{6} \tag{12}$$

$$V_{M_{BI}} = \frac{4}{3}\pi\left(1-z^2\right)^{\frac{3}{2}} - \left(\frac{4}{3}\pi\left(1-l^2\right)^{\frac{3}{2}} + V_{M_{BII}} + V_{i_{II}} + V_{i_I}\right),\ l = k_2\sin\beta' \tag{13}$$

$$V_{M_I} = \frac{4}{3}\pi\left(1-l^2\right) - V_{M_{II}},\ l = k_2\sin\beta' \tag{14}$$

where k_1 and z are model parameters. Parameters P1 in "V_j^{P1}" denotes the volume of EBM boxes located in part (II) but their volumes are calculated using parameter k_1 instead of k_2.

Consequently, the volume of EBM boxes located in part (II) can be calculated as follows:

$$V_{i_{II}} = V^{P1}_{i_{II}}|_{\beta'=f(k_2),\,k_1\to k_2} \tag{15}$$

$$V_{ii_{II}} = V^{P1}_{ii_{II}+i_{II}}|_{\beta'=f(k_2),\,k_1\to k_2} - V_{i_{II}} \tag{16}$$

$$V_{M_{II}} = V^{P1}{}_{M_{II}}|_{k_1\to k_2} \tag{17}$$

$$\begin{cases} V_{M_{CII}} = V^{P2}_{M_{CI}} = \dfrac{4\pi - 3\left(\frac{4}{3}\pi\left(1-z^2\right)^{\frac{3}{2}} + V_{N_I} + V_{N_{II}} + V^{P2}_{ii_I} + V_{ii_{II}} + V^{P2}_{a_I}\right)}{6} \\ \text{where} \begin{cases} V^{P2}_{ii_I} = V_{ii_I}|_{k_1\to k_2} \\ V^{P2}_{a_I} = V^{P2}_{ii_I} - V_{ii_{II}} \end{cases} \end{cases} \tag{18}$$

$$V_{M_{BII}} = \frac{\pi(1-\cos\beta'')^2}{3}(2+\cos\beta'') - \left(V_{M_{II}} + V_{i_{II}} + V_{M_{CII}} + V_{ii_{II}} + V_{N_{II}}\right) \tag{19}$$

where k_2 is model parameter. Parameters P2 in "V_j^{P2}" denotes

the volume of EBM boxes located in part (I) but their values are calculated using parameter k_2 instead of k_1.

Therefore, the volume fraction of EBM boxes located in part (I) can be calculated as follows:

$$\varphi_j|_{j=\mathrm{M_{BI}, i_I}} = \frac{V_j}{V_\mathrm{B}|_\mathrm{P1}}\ ,\ V_\mathrm{B}|_\mathrm{P1} = V_{\mathrm{M_{BI}}} + V_{\mathrm{i_I}} \tag{20}$$

$$\varphi_j|_{j=\mathrm{M_{CI}, ii_I, N_I, a_I}} = \frac{V_j}{V_\mathrm{C}|_\mathrm{P1}}\ ,\ V_\mathrm{C}|_\mathrm{P1} = V_{\mathrm{M_{CI}}} + V_{\mathrm{ii_I}} + V_{\mathrm{N_I}} + V_{\mathrm{a_I}} \tag{21}$$

$$\phi_\mathrm{A}|_\mathrm{P1} = \frac{3\,V_{\mathrm{M_I}}}{4\pi - \left(\pi(1-\cos\beta'')^2(2+\cos\beta'')\right)} \tag{22}$$

$$\phi_\mathrm{B}|_\mathrm{P1} = \frac{3\left(V_{\mathrm{M_I}} + V_{\mathrm{M_{BI}}} + V_{\mathrm{i_I}}\right)}{4\pi - \left(\pi(1-\cos\beta'')^2(2+\cos\beta'')\right)} \tag{23}$$

$$\phi_\mathrm{C}|_\mathrm{P1} = \frac{3\left(V_{\mathrm{N_I}} + V_{\mathrm{M_{CI}}} + V_{\mathrm{ii_I}} + V_{\mathrm{a_I}}\right)}{4\pi - \left(\pi(1-\cos\beta'')^2(2+\cos\beta'')\right)} \tag{24}$$

and the volume fraction of EBM boxes located in part (II):

$$\varphi_j|_{j=\mathrm{M_{BII}, i_{II}}} = \frac{V_j}{V_\mathrm{B}|_\mathrm{P2}}\ ,\ V_\mathrm{B}|_\mathrm{P2} = V_{\mathrm{M_{BII}}} + V_{\mathrm{i_{II}}} \tag{25}$$

$$\varphi_j|_{j=\mathrm{M_{CII}, ii_{II}, N_{II}}} = \frac{V_j}{V_\mathrm{C}|_\mathrm{P2}}\ ,\ V_\mathrm{C}|_\mathrm{P2} = V_{\mathrm{M_{CII}}} + V_{\mathrm{ii_{II}}} + V_{\mathrm{N_{II}}} \tag{26}$$

$$\phi_\mathrm{A}|_\mathrm{P2} = \frac{3\,V_{\mathrm{M_{BII}}}}{\pi(1-\cos\beta'')^2(2+\cos\beta'')} \tag{27}$$

$$\phi_\mathrm{B}|_\mathrm{P2} = \frac{3\left(V_{\mathrm{i_{II}}} + V_{\mathrm{M_{BII}}}\right)}{\pi(1-\cos\beta'')^2(2+\cos\beta'')} \tag{28}$$

$$\phi_\mathrm{C}|_\mathrm{P2} = \frac{3\left(\mathrm{V_{N_{II}}} + V_{\mathrm{ii_{II}}} + V_{\mathrm{M_{CII}}}\right)}{\pi(1-\cos\beta'')^2(2+\cos\beta'')} \tag{29}$$

Considering Eqs. (20)−(24), it is possible to calculate the tensile modulus ($E|_\mathrm{P1}$) of part (I) in EBM model using Eqs. (30)−(35):

$$E|_\mathrm{P1} = 2G|_\mathrm{P1}\,(1+\upsilon_\mathrm{co.}|_\mathrm{P1}) \tag{30}$$

where $G|_\mathrm{P1}$ and $\upsilon_\mathrm{c}|_\mathrm{P1}$ are the shear modulus and Poisson's ratio of part (I), respectively, which can be calculated using Eqs. (31)−(35):

$$G|_\mathrm{P1} = \left(\frac{\phi_\mathrm{A}|_\mathrm{P1}}{G_\mathrm{A}|_\mathrm{P1}} + \frac{\phi_\mathrm{B}|_\mathrm{P1}}{G_\mathrm{B}|_\mathrm{P1}} + \frac{\phi_\mathrm{C}|_\mathrm{P1}}{G_\mathrm{C}|_\mathrm{P1}}\right)^{-1} \tag{31}$$

where $G_\mathrm{A}|_\mathrm{P1}$, $G_\mathrm{B}|_\mathrm{P1}$, and $G_\mathrm{C}|_\mathrm{P1}$ are the shear moduli of sections A, B, and C of part (I) in EBM model, respectively.

$$G_\mathrm{A}|_\mathrm{P1} = \frac{E_\mathrm{M}|_\mathrm{P1}}{2(1+\upsilon_\mathrm{M}|_\mathrm{P1})} \tag{32}$$

where $E_\mathrm{M}|_\mathrm{P1}$ and $\upsilon_\mathrm{M}|_\mathrm{P1}$ are the modulus and the Poisson's ratio of the polymer phase occupying part (I), respectively.

$G_\mathrm{B}|_\mathrm{P1}$ can be calculated using Eqs. (33a)−(33e) as follows:

$$G_\mathrm{B}|_\mathrm{P1} = \frac{E_\mathrm{B}|_\mathrm{P1}}{2(1+\upsilon_\mathrm{B}|_\mathrm{P1})} \tag{33a}$$

$$E_\mathrm{B}|_\mathrm{P1} = \left(\frac{\varphi_{\mathrm{M_{BI}}}}{E_\mathrm{M}|_\mathrm{P1}} + \frac{\varphi_{\mathrm{i_I}}}{E_\mathrm{i}|_\mathrm{P1}}\right)^{-1} \tag{33b}$$

$$\upsilon_\mathrm{B}|_\mathrm{P1} = \upsilon_\mathrm{B}^{\mathrm{trans.}}|_\mathrm{P1}\,\frac{E_{\mathrm{B}|_\mathrm{P1}}}{E_\mathrm{B}^{\mathrm{trans.}}|_\mathrm{P1}} \tag{33c}$$

$$E_\mathrm{B}^{\mathrm{trans.}}|_\mathrm{P1} = \varphi_{\mathrm{M_{BI}}}E_\mathrm{M}|_\mathrm{P1} + \varphi_{\mathrm{i_I}}E_\mathrm{i}|_\mathrm{P1} \tag{33d}$$

$$\begin{cases} \upsilon_\mathrm{B}^{\mathrm{trans.}}|_\mathrm{P1} = \varphi_{\mathrm{M_{BI}}}\upsilon_\mathrm{M}^{\mathrm{trans.}}|_\mathrm{P1} + \varphi_{\mathrm{i_I}}\upsilon_\mathrm{i}^{\mathrm{trans.}}|_\mathrm{P1}; \\ \left(\text{Assumption}: \upsilon_\mathrm{M}^{\mathrm{trans.}}|_\mathrm{P1} = \upsilon_\mathrm{M}|_\mathrm{P1} \text{ and } \upsilon_\mathrm{i}^{\mathrm{trans.}}|_\mathrm{P1} = \upsilon_\mathrm{i}|_\mathrm{P1}\right) \end{cases} \tag{33e}$$

where $E_\mathrm{B}|_\mathrm{P1}$ and $\upsilon_\mathrm{B}|_\mathrm{P1}$ are the tensile modulus and the Poisson's ratio of the section B of EBM model, respectively. Also, $E_\mathrm{i}|_\mathrm{P1}$ and $\upsilon_\mathrm{i}|_\mathrm{P1}$ are the tensile modulus and Poisson's ratio of the polymer/particle interphase in part (I), respectively. The term "*trans*." denotes transverse direction. $G_\mathrm{C}|_\mathrm{P1}$ can be calculated in the same way:

$$G_\mathrm{C}|_\mathrm{P1} = \frac{E_\mathrm{C}|_\mathrm{P1}}{2(1+\upsilon_\mathrm{C}|_\mathrm{P1})} \tag{34a}$$

$$E_\mathrm{C}|_\mathrm{P1} = \left(\frac{\varphi_{\mathrm{M_{CI}}}}{E_\mathrm{M}|_\mathrm{P1}} + \frac{\varphi_{\mathrm{ii_I}}}{E_\mathrm{i}|_\mathrm{P1}} + \frac{\varphi_{\mathrm{N_I+a_I}}}{E_{\mathrm{N_I+a_I}}}\right)^{-1},$$

$$\begin{cases} \varphi_{\mathrm{N_I+a_I}} = \dfrac{V_{\mathrm{N_I}} + V_{\mathrm{a_I}}}{V_\mathrm{C}|_\mathrm{P1}} \\ E_{\mathrm{N_I+a_I}} = \varphi_{\mathrm{N_I}}E_\mathrm{n} + \varphi_{\mathrm{a_I}}E_\mathrm{i}|_\mathrm{P1} \end{cases} \tag{34b}$$

$$\upsilon_\mathrm{C}|_\mathrm{P1} = \upsilon_\mathrm{C}^{\mathrm{trans.}}|_\mathrm{P1}\,\frac{E_\mathrm{C}|_\mathrm{P1}}{E_\mathrm{C}^{\mathrm{trans.}}|_\mathrm{P1}} \tag{34c}$$

$$E_\mathrm{C}^{\mathrm{trans.}}|_\mathrm{P1} = \varphi_{\mathrm{M_{CI}}}E_\mathrm{M}|_\mathrm{P1} + \varphi_{\mathrm{N_I+a_I}}E_{\mathrm{N_I+a_I}} + \varphi_{\mathrm{ii_I}}E_\mathrm{i}|_\mathrm{P1} \tag{34d}$$

$$\begin{cases} \upsilon_\mathrm{C}^{\mathrm{trans.}}|_\mathrm{P1} = \varphi_{\mathrm{M_{CI}}}\upsilon_\mathrm{M}^{\mathrm{trans.}}|_\mathrm{P1} + \varphi_{\mathrm{N_I+a_I}}\upsilon_{\mathrm{N_I+a_I}}^{\mathrm{trans.}} + \varphi_{\mathrm{ii_I}}\upsilon_\mathrm{i}^{\mathrm{trans.}}|_\mathrm{P1} \\ \left(\text{Assumptions}: \upsilon_\mathrm{M}^{\mathrm{trans.}}|_\mathrm{P1} = \upsilon_\mathrm{M}|_\mathrm{P1} \text{ and } \upsilon_\mathrm{i}^{\mathrm{trans.}}|_\mathrm{P1} = \upsilon_\mathrm{i}|_\mathrm{P1}\right) \end{cases} \tag{34e}$$

$$\upsilon_{\mathrm{N_I+a_I}}^{\mathrm{trans.}} = \upsilon_{\mathrm{N_I+a_I}}\,\frac{E_{\mathrm{N_I+a_I}}^{\mathrm{trans.}}}{E_{\mathrm{N_I+a_I}}} \tag{34f}$$

$$E_{\mathrm{N_I+b_I}}^{\mathrm{trans.}} = \left(\frac{\varphi_{\mathrm{N_I}}}{E_\mathrm{n}} + \frac{\varphi_{\mathrm{a_I}}}{E_\mathrm{i}^{\mathrm{trans.}}|_\mathrm{P1}}\right)^{-1},$$

$$\left(\text{Assumption}: E_\mathrm{i}^{\mathrm{trans.}}|_\mathrm{P1} = E_\mathrm{i}|_\mathrm{P1}\right) \tag{34g}$$

$$\upsilon_{\mathrm{N_I+a_I}} = \varphi_{\mathrm{N_I}}\upsilon_\mathrm{n} + \varphi_{\mathrm{a_I}}\upsilon_\mathrm{i}|_\mathrm{P1} \tag{34h}$$

where $E_\mathrm{C}|_\mathrm{P1}$ and $\upsilon_\mathrm{C}|_\mathrm{P1}$ are the tensile modulus and the Poisson's ratio of the section C of EBM model, respectively. E_n and υ_n denote the tensile modulus and Poisson's ration of the applied Janus nanoparticles, respectively.

https://doi.org/10.1007/s10118-019-2178-3

$$\upsilon_{co.}|_{P1} = \phi_{nan.}|_{P1}\upsilon_n + \phi_{int.}|_{P1}\upsilon_i|_{P1} + \phi_{polym.}|_{P1}\upsilon_M|_{P1} \quad (35a)$$

$$\phi_{int.}|_{P1} = \frac{\frac{4}{3}\pi\left(k_1{}^3 - z^3\right) - \left(V_{i_{II}}^{P1} + V_{ii_{II}}^{P1}\right)}{\frac{4}{3}\pi - \left(\frac{\pi(1-\cos\beta'')^2}{3}(2+\cos\beta'')\right)} \quad (35b)$$

$$\phi_{polym.}|_{P1} = \frac{\frac{4}{3}\pi\left(1 - k_1{}^3\right) - \left(V_{M_{II}}^{P1} + V_{M_{BII}}^{P1} + V_{M_{CII}}^{P1} + V_{b_I}\right)}{\frac{4}{3}\pi - \left(\frac{\pi(1-\cos\beta'')^2}{3}(2+\cos\beta'')\right)} \quad (35c)$$

$$\phi_{nan.}|_{P1} = \frac{V_{N_I}}{\frac{4}{3}\pi - \left(\frac{\pi(1-\cos\beta'')^2}{3}(2+\cos\beta'')\right)} \quad (35d)$$

Considering Eqs. (25)–(29), it is possible to calculate the tensile modulus of part (II) ($E|_{P2}$) of EBM model using Eqs. (36)–(41):

$$E|_{P2} = 2G|_{P2}(1+\upsilon_{co.}|_{P2}) \quad (36)$$

where $G|_{P2}$ and $\upsilon_c|_{P2}$ are the shear modulus and Poisson's ratio of the part (II), respectively, which can be calculated using Eqs. (37)–(40):

$$G|_{P2} = \left(\frac{\phi_A|_{P2}}{G_A|_{P2}} + \frac{\phi_B|_{P2}}{G_B|_{P2}} + \frac{\phi_C|_{P2}}{G_C|_{P2}}\right)^{-1} \quad (37)$$

where $G_A|_{P2}$, $G_B|_{P2}$, and $G_C|_{P2}$ are the shear modulus of sections A, B, and C of part (II) of EBM model, respectively.

$$G_A|_{P2} = \frac{E_M|_{P2}}{2(1+\upsilon_M|_{P2})} \quad (38)$$

where $E_M|_{P2}$ and $\upsilon_M|_{P2}$ are the modulus and the Poisson's ratio of the polymer phase occupying part (II), respectively.

$G_B|_{P2}$ can be calculated using Eqs. (39a)–(39e) as follows:

$$G_B|_{P2} = \frac{E_B|_{P2}}{2(1+\upsilon_B|_{P2})} \quad (39a)$$

$$E_B|_{P2} = \left(\frac{\varphi_{i_{II}}}{E_i|_{P2}} + \frac{\varphi_{M_{BII}}}{E_M|_{P2}}\right)^{-1} \quad (39b)$$

$$\upsilon_B|_{P2} = \upsilon_B^{trans.}|_{P2}\frac{E_B|_{P2}}{E_B^{trans.}|_{P2}} \quad (39c)$$

$$E_B^{trans.}|_{P2} = \varphi_{M_{BII}}E_M|_{P2} + \varphi_{i_{II}}E_i|_{P2} \quad (39d)$$

$$\begin{cases} \upsilon_B^{trans.}|_{P2} = \varphi_{M_{BII}}\upsilon_M^{trans.}|_{P2} + \varphi_{i_{II}}\upsilon_i^{trans.}|_{P2}; \\ \left(\text{Assumption}: \upsilon_M^{trans.}|_{P2} = \upsilon_M|_{P2} \text{ and } \upsilon_i^{trans.}|_{P2} = \upsilon_i|_{P2}\right) \end{cases} \quad (39e)$$

where $E_B|_{P2}$ and $\upsilon_B|_{P2}$ are the tensile modulus and the Poisson's ratio of the section B of EBM model, respectively. Also, $E_i|_{P2}$ and $\upsilon_i|_{P2}$ are the tensile modulus and Poisson's ratio of the polymer/particle interphase in part (II), respectively. The term "*trans.*" denotes transverse direction. Consequently, $G_C|_{P2}$ can be calculated as follows:

$$G_C|_{P2} = \frac{E_C|_{P2}}{2(1+\upsilon_C|_{P2})} \quad (40a)$$

$$E_C|_{P2} = \left(\frac{\varphi_{M_{CII}}}{E_M|_{P2}} + \frac{\varphi_{ii_{II}}}{E_i|_{P2}} + \frac{\varphi_{N_{II}}}{E_n}\right)^{-1} \quad (40b)$$

$$\upsilon_C|_{P2} = \upsilon_C^{trans.}|_{P2}\frac{E_C|_{P2}}{E_C^{trans.}|_{P2}} \quad (40c)$$

$$E_C^{trans.}|_{P2} = \varphi_{M_{CII}}E_M|_{P2} + \varphi_{N_{II}}E_n + \varphi_{ii_{II}}E_i|_{P2} \quad (40d)$$

$$\begin{cases} \upsilon_C^{trans.}|_{P2} = \varphi_{M_{CII}}\upsilon_M^{trans.}|_{P2} + \varphi_{N_{II}}\upsilon_n^{trans.} + \varphi_{ii_{II}}\upsilon_i^{trans.}|_{P2} \\ \left(\text{Assumptions}: \upsilon_M^{trans.}|_{P2} = \upsilon_M|_{P2} \text{ and } \upsilon_i^{trans.}|_{P2} = \upsilon_i|_{P2}\right) \\ \text{and } \upsilon_n^{trans.} = \upsilon_n\Big) \end{cases} \quad (40e)$$

where $E_C|_{P2}$ and $\upsilon_C|_{P2}$ are the tensile modulus and the Poisson's ratio of the section C of EBM model, respectively.

$$\upsilon_{co.}|_{P2} = \phi_{nan.}|_{P2}\upsilon_n + \phi_{int.}|_{P2}\upsilon_i|_{P2} + \phi_{polym.}|_{P2}\upsilon_M|_{P2} \quad (41a)$$

$$\phi_{int.}|_{P2} = \frac{\frac{4}{3}\pi\left(k_2{}^3 - z^3\right) - \left(V_{i_I}^{P2} + V_{ii_I}^{P2} + V_{a_I}^{P2}\right)}{\frac{\pi(1-\cos\beta'')^2}{3}(2+\cos\beta'')}, \quad V_{a_I}^{P2} = V_{ii_I}^{P2} - V_{ii_{II}} \quad (41b)$$

$$\phi_{polym.}|_{P2} = \frac{\frac{4}{3}\pi\left(1 - k_1{}^3\right) - \left(V_{M_I}^{P2} + V_{M_{BI}}^{P2} + V_{M_{CI}}^{P2} + V_{b_I}^{P2}\right)}{\frac{\pi(1-\cos\beta'')^2}{3}(2+\cos\beta'')}, \quad V_{b_I}^{P2} = V_{M_{BI}}^{P2} - V_{M_{BII}} \quad (41c)$$

$$\phi_{nan.}|_{P2} = \frac{V_{N_{II}}}{\frac{\pi(1-\cos\beta'')^2}{3}(2+\cos\beta'')} \quad (41d)$$

Finally, combination of Eqs. (30) and (36) results in Eq. (42a) which predicts the tensile modulus of polymer/polymer interface region ($E_{In.}$):

$$E_{In.} = \left(\frac{\phi_{part\ (I)}}{E_{P1}} + \frac{\phi_{part\ (II)}}{E_{P2}}\right)^{-1} \quad (42a)$$

$$\phi_{part\ (I)} = 1 - 0.25\left((1-\cos\beta'')^2(2+\cos\beta'')\right) \quad (42b)$$

$$\phi_{part\ (II)} = 0.25\left((1-\cos\beta'')^2(2+\cos\beta'')\right) \quad (42c)$$

Parameters z, k_1, and k_2 can be calculated by applying NAS model to nanocomposite comprising phase (I) and nanoparticles with similar surface chemistry to Janus surface section (A) (Fig. 1b) and nanocomposite comprising phase (II) and nanoparticles with similar surface chemistry to Janus surface section (B) as follows:

$$z = \sqrt[3]{\frac{\phi_d}{w}} \quad (43)$$

$$k_1 = \sqrt[3]{\frac{\phi_d}{w}\left(1 + \frac{1}{8w}\left(\frac{(r+\tau_1)^3}{r^3} - 1\right)\right)} \quad (44a)$$

$$k_2 = \sqrt[3]{\frac{\phi_d}{w}\left(1+\frac{1}{8w}\left(\frac{(r+\tau_2)^3}{r^3}-1\right)\right)} \quad (44b)$$

where r is the radius of an individual spherical Janus nanoparticle, τ_1 and τ_2 are the thicknesses of polymer/particle interphases, respectively, w indicates the numerical correlation between the model and actual system, ϕ_d is the actual volume fraction of Janus nanoparticles in the polymer/polymer interface region.[31] Furthermore, $E_i|_{P1}$ and $E_i|_{P2}$ should be calculated based on the linear variation of the modulus in polymer/particle interphase in $\bar{r}$ direction:

$$E_i(a)|_{P1} = E_i(0)|_{P1} + \frac{E_M|_{P1} - E_i(0)|_{P1}}{k_1 - z}(a-z) \quad (45a)$$

$$\frac{1}{E_i|_{P1}} = \frac{3}{(k_1{}^2 - z^2)}\int_z^{k_1}\frac{a^2 da}{E_i(a)|_{P1}} \quad (45b)$$

$$E_i(a)|_{P2} = E_i(0)|_{P2} + \frac{E_M|_{P2} - E_i(0)|_{P2}}{k_2 - z}(a-z) \quad (46a)$$

$$\frac{1}{E_i|_{P2}} = \frac{3}{(k_2{}^2 - z^2)}\int_z^{k_1}\frac{a^2 da}{E_i(a)|_{P2}} \quad (46b)$$

where $E_i(0)|_j$ is the modulus of polymer/particle interphase on the surface of Janus nanoparticles. Parameters τ_1, τ_2, and $E_i(0)|_j$ should be necessarily determined using the combination of NAS model and the results of tensile test (which will be discussed later).[31] It should be noted that the modeling procedures regarding to the cases $k_1 > k_2$ and $k_1 = k_2$ are presented in ESI (S2 and S3).

Modeling of BBN System (KAd Model)

In this step, the whole BBN system is simulated as a developed geometrical structure based on the model proposed by Kolarik *et al.*[32,45] The volume fraction range of dispersed polymer phase ($\bar{\phi}_2$) is divided into four separated intervals based on the percolation thresholds of phase (I) (ϕ_{cr1}), phase (II) (ϕ_{cr2}), and also phases inversion point ($\phi_{pi.}$). Consequently, the modeling procedure should be performed in the following intervals and also at phase inversion point:

1. First interval: $(0 \leqslant \bar{\phi}_2 \leqslant \phi_{cr2})$
2. Second interval: $(\phi_{cr2} \leqslant \bar{\phi}_2 < \phi_{pi.})$
3. Phase inversion point: $\bar{\phi}_2 = \phi_{pi.}$
4. Third interval: $(\phi_{pi} < \bar{\phi}_2 \leqslant 1 - \phi_{cr1})$
5. Fourth interval: $(1 - \phi_{cr1} < \bar{\phi}_2 \leqslant 1)$

It is notable that the actual blend morphology in the first and fourth intervals is droplet-matrix, in the second and third intervals is a combination of droplet-matrix and co-continuous (caused by the interconnection of droplets) morphologies, and at the phase inversion point is completely co-continuous.[44] As illustrated in Fig. 5, this concept is fully considered in designing the structure of KAd model based on the model proposed by Wang *et al.*[44]

Modeling at phase inversion point

The hypothetical geometrical structure is of KAd model at phase inversion point depicted in Fig. 6 which is corresponding to the co-continuous morphology.[44,48]

Accordingly, the tensile modulus of BBN system at phase inversion point can be calculated using Eqs. (47a)−(47g):

$$E_{BBN}|_{pi} = \left(\phi_{2p}E_M|_{P2} + \phi_{1p}E_M|_{P1} + \phi_{In.p}E_{In.}\right) + \frac{(\phi_{1s}+\phi_{2s}+\phi_{In.s})^2}{\left(\frac{\phi_{1s}}{E_M|_{P1}} + \frac{\phi_{2s}}{E_M|_{P2}} + \frac{\phi_{In.s}}{E_{In.}}\right)} \quad (47a)$$

$$\phi_{2s} = 2\pi r_P{}^2 - 2\left(16 - \sqrt{128}\right)r_P{}^3 \quad (47b)$$

$$\phi_{1s} = 4\left(R - R^2\right) - \left(3\pi R^2 - 2\left(16 - \sqrt{128}\right)R^3\right) \quad (47c)$$

$$\phi_{In.s} = 2\pi R^2 - 2\left(16 - \sqrt{128}\right)R^3 - \phi_{2s} \quad (47d)$$

$$\phi_{2p} = \pi r_P{}^2 \quad (47e)$$

$$\phi_{In.p} = \pi\left(R^2 - r_P{}^2\right) \quad (47f)$$

$$\phi_{1p} = 1 - \left(\phi_{2s} + \phi_{1s} + \phi_{In.s} + \phi_{2p} + \phi_{In.p}\right) \quad (47g)$$

where $E_{In.}$ can be calculated using Eq. (42a), parameters r_p and R are model parameters (Fig. 6b).

It is very important to determine the share of each poly-

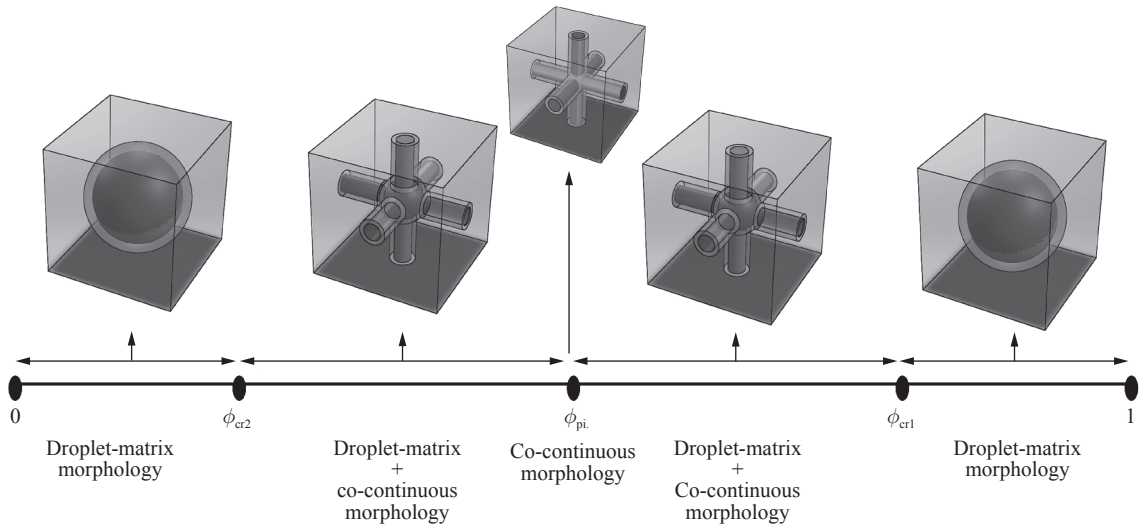

Fig. 5 Geometrical structure of KAd model corresponding to the actual blend morphology in different intervals plus phase inversion point

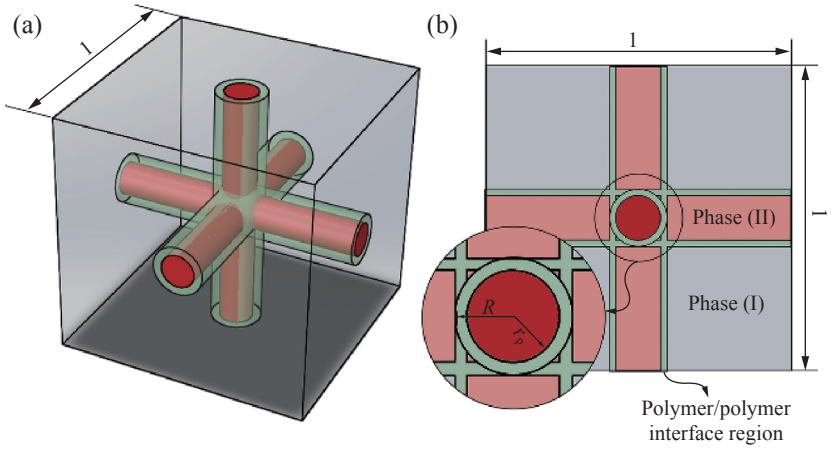

Fig. 6 (a) Geometrical structure of KAd model at phase inversion point and (b) the side view of the structure. The whole structure is surrounded by a cube of unite side length.

mer phase in polymer/polymer interface region (section Modeling of polymer/polymer interface region) in which Janus nanoparticles are placed at polymer/polymer interface (Fig. 2). This leads to determination of the thickness of polymer/polymer interface region as well as parameters r_p and R. Therefore, it is considered that a percentage of the volume fraction of each polymer phase (y_p) participates in the interface region, so:

$$\bar{\phi}_2' = \bar{\phi}_2 \times y_p \tag{48}$$

$$\bar{\phi}_1' = \bar{\phi}_1 \times y_p \tag{49}$$

where $\bar{\phi}_1'$ and $\bar{\phi}_2'$ are the volume fractions of the participant portions of phase (I) and phase (II) in the interface region, respectively, $\bar{\phi}_1$ and $\bar{\phi}_2$ denote the actual (experimental) volume fractions of phases (I) and (II), respectively. Applying Eqs. (47b) and (47e), it is now possible to calculate parameter r_p as follows:

$$\begin{cases} f(r_p) = \phi_{pi.}\left(1-(y_p)\right) - 3\pi r_p + 2\left(16+\sqrt{128}\right) r_p{}^3 = 0 \\ f(r_p) \to r_p \end{cases} \tag{50}$$

where $\phi_{pi.}$ is the volume fraction of phase (II) corresponding to phase inversion point.

Similarly, parameter R can be calculated using Eq. (51):

$$\begin{cases} f(R, r_p) = \phi_{In.s} + \phi_{In.p} - \left(\bar{\phi}_1' + \bar{\phi}_2' + \bar{\phi}_n\right) = 0 \\ f(R, r_p) \to R \end{cases} \tag{51}$$

where, $\bar{\phi}_n$ is the actual (experimental) volume fraction of the applied Janus nanoparticles.

As illustrated in Fig. 6, the thickness of polymer/polymer interface region (T) is equal to $R - r_p$ which is constant and independent of the volume fraction of polymer phases.

Modeling in the 2nd and 3rd intervals

The hypothetical geometrical structure of KAd model in the second and third intervals is illustrated in Fig. 7. As shown clearly, the model represents both droplet-matrix and co-continuous morphologies corresponding to the actual BBN morphology in the 2nd and 3rd intervals.[44]

The tensile modulus of BBN system in the 2nd and 3rd intervals can be calculated using Eqs. (52a)−(52h).

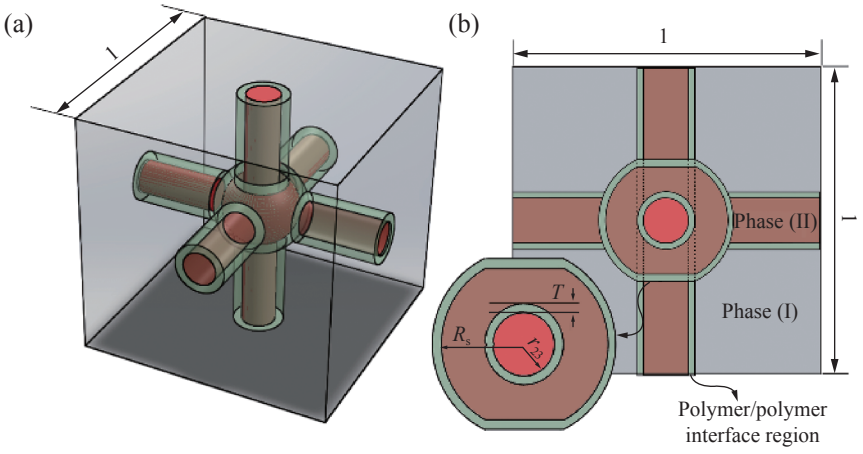

Fig. 7 (a) Geometrical structure of KAd model in the second and third intervals and (b) the side view of the structure. The whole structure is surrounded by a cube of unite side length.

https://doi.org/10.1007/s10118-019-2178-3

$$E_{\mathrm{BBN}|2,3}=\left(\phi_{2\mathrm{p}}E_{\mathrm{M}|\mathrm{P2}}+\phi_{\mathrm{In.p}}E_{\mathrm{In.}}\right)+\frac{\left(\phi_{1\mathrm{s}}+\phi_{2\mathrm{s}}+\phi_{\mathrm{In.s}}\right)^2}{\left(\frac{\phi_{1\mathrm{s}}}{E_{\mathrm{M}|\mathrm{P1}}}+\frac{\phi_{2\mathrm{s}}}{E_{\mathrm{M}|\mathrm{P2}}}+\frac{\phi_{\mathrm{In.s}}}{E_{\mathrm{In.}}}\right)}+\cdots\frac{E_{\mathrm{M}|\mathrm{P1}}\phi_{1\mathrm{c}}+E_{\mathrm{M}|\mathrm{P2}}\phi_{2\mathrm{d}}\frac{3E_{\mathrm{M}|\mathrm{P1}}}{2E_{\mathrm{M}|\mathrm{P1}}+E_{\mathrm{M}|\mathrm{P2}}}}{\phi_{1\mathrm{c}}+\phi_{2\mathrm{d}}\frac{3E_{\mathrm{M}|\mathrm{P1}}}{2E_{\mathrm{M}|\mathrm{P1}}+E_{\mathrm{M}|\mathrm{P2}}}} \tag{52a}$$

$$\phi_{2\mathrm{p}}=\pi r_{23} \tag{52b}$$

$$\phi_{\mathrm{In.p}}=\pi\left(R^2-{r_{23}}^2\right) \tag{52c}$$

$$\phi_{2\mathrm{s}}=2\left(\pi{r_{23}}^2-\left(\frac{4}{3}\pi(R_{\mathrm{s}}+T)^3-2\pi h\left((R_{\mathrm{s}}+T)^2-\frac{\left(R_{\mathrm{s}}\cos\left(\arcsin\left(\frac{r_{23}}{R_{\mathrm{s}}+T}\right)\right)\right)}{3}-r_{23}\right)\right)\right) \tag{52d}$$

$$\begin{cases}\phi_{1\mathrm{s}}=4\left(2\left(r_{23}+T\right)(0.5-h)-\frac{\phi_{2\mathrm{s}}}{4}-\frac{\pi h^2}{3}\left(3\left(R_{\mathrm{s}}+T\right)-h\right)\right)\\ \text{where } h=(R_{\mathrm{s}}+T)\left(1-\cos\left(\arcsin\left(\frac{r_{23}+T}{R_{\mathrm{s}}+T}\right)\right)\right)\end{cases} \tag{52e}$$

$$\begin{cases}\phi_{\mathrm{In.s}}=2\left(\pi(r_{23}+T)^2-\left(2\pi h_1(R_{\mathrm{s}}+T)^2-\frac{{h_1}^2}{3}-(r_{23}+T)+2\pi h_1(R_{\mathrm{s}}+T)^2-\frac{{h_2}^2}{3}-r_{23}\right)\right)\\ \text{where }\begin{cases}h_1=(R_{\mathrm{s}}+T)\cos\left(\arcsin\left(\frac{r_{23}+T}{R_{\mathrm{s}}+T}\right)\right)\\ h_2=(R_{\mathrm{s}}+T)\cos\left(\arcsin\left(\frac{r_{23}}{R_{\mathrm{s}}+T}\right)\right)\end{cases}\end{cases} \tag{52f}$$

$$\phi_{2\mathrm{d}}=\frac{4}{3}\pi\left({R_{\mathrm{s}}}^2-(r_{23}+T)^2\right)^{\frac{3}{2}} \tag{52g}$$

$$\phi_{1\mathrm{c}}=1-\left(\phi_{2\mathrm{d}}+\phi_{\mathrm{In.s}}+\phi_{1\mathrm{s}}+\phi_{2\mathrm{s}}+\phi_{\mathrm{In.p}}+\phi_{2\mathrm{p}}\right) \tag{52h}$$

where T is the thickness of polymer/polymer interface region which is calculated in section Modeling at phase inversion point, r_{23} and R_{s} are the model parameters at the 2nd and 3rd intervals (Fig. 7b). Parameter r_{23} can be calculated using r_{p} (Eq. 50) as follows:

$$r_{23}=r_{\mathrm{p}}\times R(D)\ ;\ R(D)=\frac{\bar{\phi}_2-\left(\bar{\phi}_2'+\phi_{\mathrm{cr2}}\right)}{\phi_{\mathrm{pi.}}\left(1-\left(y_{\mathrm{p}}\right)\right)-\phi_{\mathrm{cr2}}} \tag{53}$$

where $R(D)$ is a developed form of the parameter used by Wang *et al.* in order to make correlation between their proposed model structures for the 2nd/3rd interval and phase inversion point.[44] Considering constant T, it is possible to determine R_{s} using Eqs. (52b), (52d), and (52g):

$$\begin{cases}f(R_{\mathrm{s}},r_{23})=\bar{\phi}_2-\bar{\phi}_2'-\left(\phi_{2\mathrm{p}}+\phi_{2\mathrm{s}}+\phi_{2\mathrm{d}}\right)=0\\ f(R_{\mathrm{s}},r_{23})\rightarrow R_{\mathrm{s}}\end{cases} \tag{54}$$

Modeling in the 1st and 4th intervals

The hypothetical geometrical structure of KAd model in the first and fourth intervals is depicted in Fig. 8. As shown clearly, the model structure in these two intervals is a developed form of Maxwell-Eucken model which includes

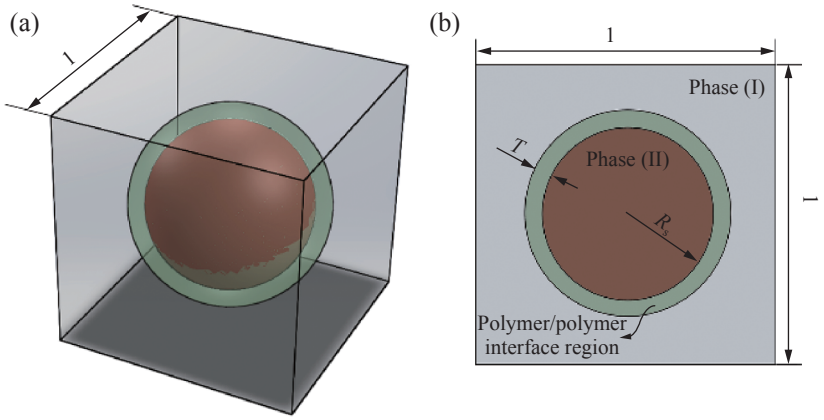

Fig. 8 (a) Geometrical structure of KAd model in the first and fourth intervals and (b) the side view of the structure. The whole structure is surrounded by a cube of unite side length.

https://doi.org/10.1007/s10118-019-2178-3

added polymer/polymer interface region (Fig. 8b) and upgraded governing equations.[44]

Accordingly, model parameter R_s can be determined using Eq. (55):

$$\bar{\phi}_2 - \bar{\phi}'_2 = \frac{4}{3}\pi {R_s}^3 \tag{55}$$

As a result, the tensile modulus of BBN system in the 1st and 4th intervals can be calculated using Eqs. (56a)−(56g):

$$E_{BBN}|_{1,4} = \frac{E_M|_{P1}\phi'_1 + E'_M\phi'_2\dfrac{3E_M|_{P1}}{2E_M|_{P1}+E'_M}}{\phi'_1 + \phi'_2\dfrac{3E_M|_{P1}}{2E_M|_{P1}+E'_M}} \tag{56a}$$

$$\phi'_1 = \phi_1\left(1-\left(y_p\right)\right) \tag{56b}$$

$$\phi'_2 = \phi_{In.} + \phi_2\left(1-\left(y_p\right)\right) \tag{56c}$$

$$\phi_{In.} = \frac{4}{3}\pi\left((R_s+T)^3 - {R_s}^3\right) \tag{56d}$$

$$\phi_1 = 1-(\phi_2 - \phi_{In.}) \tag{56e}$$

$$\phi_2 = \frac{4}{3}\pi {R_s}^3 \tag{56f}$$

$$E'_2 = \left(\frac{\phi_2\left(1-\left(y_p\right)\right)}{E_M|_{P2}} + \frac{\phi_{In.}}{E_{In.}}\right)^{-1} \tag{56g}$$

EXPERIMENTAL

Materials

Paraffin (Dr. Mojallali Industrial Chemical Complex Co., Laboratory grade) was used as oil phase (in Pickering emulsions) with a very narrow range of melting temperature from 56 °C to 58 °C and density of 0.9 g/cm^3. (3-Aminopropyl)triethoxysilane (APTES, Aldrich, 99%), methanol (Dr. Mojallali Industrial Chemical Complex Co., > 99%), chloroform (Dr. Mojallali Industrial Chemical Complex Co., > 99%), ethanol (Merck, 99.9%), hexadecyltrimethoxysilane (HDTMS, Aldrich, ≥ 85%), and dichloromethane (Merck, 99.9%) were used as received. Solid-stabilized emulsions (Pickering emulsions) were obtained using hydrophilic silica nanoparticles (Aerosil fumed silica, P1 (OX-50): d = 40 nm) provided kindly by Degussa. Their characteristics are reported in ESI (Section S4: Table S4-1 and Fig. S4-1). Polystyrene (PS) (Grade 1160 GPPS) was purchased from Tabriz Petrochemical Corporation and poly(methyl methacrylate) (Grade EG920) was purchased from LG Corporation.

Preparation of Janus Nanoparticles

The applied Janus nanoparticles in this investigation were prepared based on the method described in our previous work.[46] P1 silica nanoparticles (4 g) were dispersed in deionized water (4 L) using a mixer at 2500 r/min for 20 min and heated to 65 °C. Paraffin (450 g) was added to the mixture and allowed to completely melt down. Thereafter, the system was stirred by an industrial mixer (at 2800 r/min for 1 h). After mixing stage, emulsions were immediately poured into a cold water bath (5 °C) to form a stabilized suspension containing solidified paraffin droplets (SPDs).

Primary modification stage

The stabilized suspension containing SPDs (covered with silica nanoparticles) was exposed to a modification process in order to functionalize the unprotected surface of silica nanoparticles. To this end, SPDs were primarily washed several times with deionized water (5 °C) to remove unattached nanoparticles as well as weakly attached ones. Thereafter, paraffin droplets were dispersed in (3-aminopropyl) triethoxysilane (APTES)/ethanol (4 L) solution for 24 h at room temperature under stirring. Thereafter, SPDs were filtrated and washed several times with methanol to remove unreacted APTES molecules. Then, SPDs were dissolved in chloroform to remove paraffin. Finally, Janus nanoparticles were collected by centrifugation and dried under vacuum for 24 h.

Secondary modification stage

In this stage, the collected Janus nanoparticles from primary modification stage ("Primary modification stage" section) were dispersed in a mixture of 0.2 vol% HDTMS in ethanol. The system was stirred at 500 r/min for 24 h at 25 °C. The final produced Janus nanoparticles were washed several times with methanol to remove unattached HDTMS molecules and then collected by centrifugation. The drying process was also performed under vacuum for 24 h.

Preparation of Uniformly Modified Nanoparticles

P1 nanoparticles were added to mixtures of ethanol (100 mL)/APTES (4 mL) and ethanol (100 mL)/HDTMS (4 mL) under stirring for 24 h. The uniformly modified nanoparticles (non-Janus) of each system were then washed several times with methanol and collected by centrifugation. It should be noted that P1 nanoparticles uniformly modified with APTES and HDTMS are referred to as UAP1 sand UHP1 nanoparticles, respectively.

Preparation of BBN and PS/PMMA Blend Samples

PS/PMMA (85/15, 60/40, 40/60, and 50/50 *V*/*V*) blend samples were prepared *via* solution mixing. For preparing blend samples containing Janus and UAP1 nanoparticles, at the first step, PMMA (15 vol% of PS/PMMA blend) was dissolved in dichloromethane till complete dissolution, nanoparticles (1 vol%, 2 vol%, 3 vol%, and 4 vol%) were added under agitation. Similarly, UHP1 nanoparticles (1 vol%, 2 vol%, 3 vol%, and 4 vol%) were added into PS (85 vol% of PS/PMMA blend)/dichloromethane solution. After 45 min, the second polymer phase was added and completely dissolution-mixed for 45 min. Thereafter, the samples were casted in a glass petri dish for 7 days at room temperature and then they were held under vacuum at 60 °C for 48 h in order to evaporate the remaining solvent.

Preparation of PS and PMMA Nanocomposites

Primarily, PS was dissolved in dichloromethane and then UAP1 nanoparticles (1 vol%, 2 vol%, 3 vol%, and 4 vol%) were added into it. The same process was performed for PMMA/UHP1 nanoparticles. The solution samples were mixed for 1 h and then casted in glass petri dish for 7 days at room temperature and then they were held under vacuum at

https://doi.org/10.1007/s10118-019-2178-3

60 °C for 48 h in order to evaporate the remaining solvent. These samples were used to determine the thicknesses of polymer/particle interphases (in PS and PMMA phases) based on the results of NAS model.

Mechanical Properties

All prepared samples were compression molded into suitable pieces for tensile tests. Molding was carried out at 180 °C followed by slow water-cooling under 10 MPa. Tensile tests were conducted on a Zwick/Roell tensile testing machine (Z 010) at a fixed crosshead speed of 5 mm/min at room temperature according to ISO 527. At least five specimens were tested for each composition and the resulting tensile properties were averaged.

RESULTS AND DISCUSSION

Fig. 9 presents a flowchart expressing the procedure of KAd model for predicting the tensile modulus of a BBN system.

At the first step, it is essential to determine parameter β (Eq. 1) which drastically affects all parts of KAd model. In our previous work, β was precisely measured for P1 nanoparticles, which was reported as 35.72°.[47] It was also proved that in a PS/PMMA blend samples, UAP1 and UHP1 nanoparticles tend to migrate toward PS and PMMA phases, respectively, while Janus nanoparticles fix at polymer/polymer interface.[20] Accordingly, it is assumed that each surface section of the synthesized Janus nanoparticles (on which APTES or HDTMS molecules are bonded) (Fig. 1b) tends to accommodate with its corresponding polymer phase and therefore the three-phase contact angle (β) at polymer/polymer interface (Fig. 2a) is equal to the predicted β using Eq. (1) (Fig. 1b).

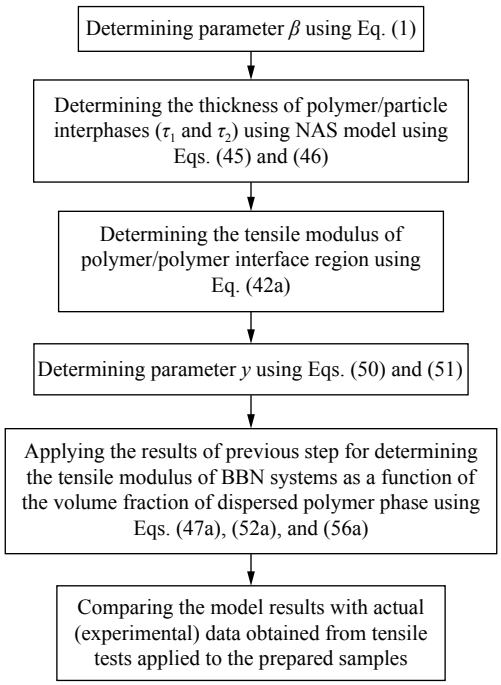

Fig. 9 The flowchart summarizing different stages of KAd model

The second step involves determining the thicknesses of polymer/particle interphases (τ_1 and τ_2) (Fig. 4). To this end, PMMA/UHP1 and PS/UAP1 nanocomposites were prepared based on the method described in section Preparation of PS and PMMA nanocomposites and the molded samples were exposed to tensile tests (section Mechanical properties). Consequently, it was possible to determine the thicknesses of polymer/particle interphases in PS and PMMA using the combination of NAS model and results of tensile tests (Table 1).[38] NAS model was also used to calculate the modulus of polymer/particle interphases on the surface of UHP1 and UAP1 nanoparticles ($E_i(0)$) which are required to define the linear variation of interphase moduli (Eq. 45a−46b) (Table 1). The tensile modulus of PMMA and PS phases were also measured based on the method described in section Mechanical properties (Table 1).

The results of the tensile test and also the predictions of KAd model for BBN samples comprising PS/PMMA (85/15 *V*/*V*) and Janus nanoparticles (1 vol%, 2 vol%, 3 vol%, and 4 vol%) are depicted in Fig. 10. As expected, the tensile modulus of BBN samples increases with the content of Janus nanoparticles up to 3 vol% and the modulus drop at 4 vol% maybe attributed to the negative effects of Janus nanoparticle agglomeration. Besides, the model predictions up to 3 vol% of Janus nanoparticles are acceptably close to the experimental results (predicting error < 8.5%), which verifies

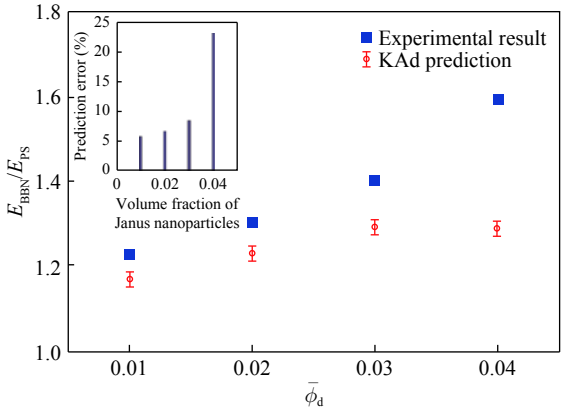

Fig. 10 Experimental results versus predictions of KAd model for BBN samples comprising PS/PMMA (85/15 *V*/*V*) and Janus nanoparticles (1 vol%, 2 vol%, 3 vol%, and 4 vol%). ϕ_{pi}, ϕ_{cr2} and $1-\phi_{cr1}$ are considered to be 0.5, 0.17 and 0.83 (vol%), respectively, and parameter $y_p = 0.48\%$ (Eqs. 48 and 49). The prediction errors of the model corresponding to each test result are also presented.

Table 1 Thickness of polymer/particle interphases in PS and PMMA phases, modulus of polymer/particle interphases on the surface of UAP1 and UAP1 nanoparticles ($E_i(0)$), the measured tensile modulus for PS and PMMA phases

	τ (m)	$E_i(0)/E_m$
PMMA/UHP1	$(1.82 \pm 0.11) \times 10^{-7}$	7.3
PS/UAP1	$(1.97 \pm 0.08) \times 10^{-8}$	6.2
E_{PS} = 2.73 (Gpa), υ_{PS} = 0.325−0.33, E_{PMMA} = 3.11 (Gpa), υ_{PS} = 0.34−0.4		

https://doi.org/10.1007/s10118-019-2178-3

the capability of KAd model to predict the tensile moduli of BBN systems comprising low contents of nanoparticles.

As described in section Preparation of BBN and PS/PMMA blend samples, some PS/PMMA blend samples (60/40, 40/60, 50/50 *V*/*V*) were also prepared in order to perform a comparison with BBN samples comprising the similar content of PS/PMMA phases and 1 vol% of Janus nanoparticles. This comparison was a good benchmark to investigate the effects of Janus nanoparticles' presence at polymer/polymer interface on PS/PMMA blend and also the model performance as a function of volume fraction of the dispersed polymer phase. As depicted in Fig. 11, the tensile modulus of BBN samples increases with the content of PMMA phase.

Besides, the presence of Janus nanoparticles at polymer/polymer interface increases the tensile modulus of BBN samples compared to their corresponding blend samples. Fig. 12 depicts the results of KAd model for simultaneous variation of the contents of dispersed polymer phase and Janus nanoparticles in PS/PMMA/Janus BBN system.

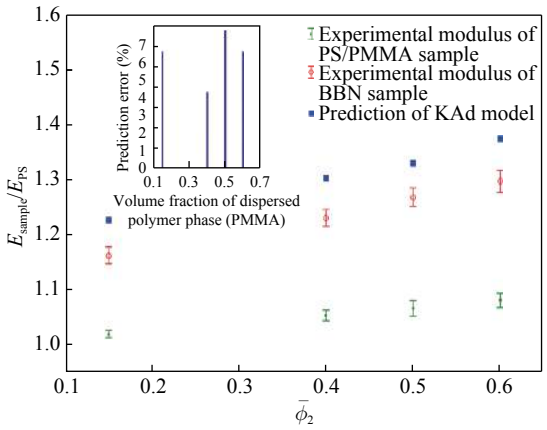

Fig. 11 Comparison of the tensile modulus of PS/PMMA samples comprising different contents of PMMA with similar BBN samples comprising 1 vol% of Janus nanoparticles. The results of KAd model for the different contents of dispersed polymer phase (PMMA) are also presented. $\bar{\phi}_n$, $\phi_{pi.}$, ϕ_{cr2} and $1-\phi_{cr1}$ are considered to be 0.1, 0.5, 0.17 and 0.83 (vol%), respectively, and parameter y_p = 0.48% (Eqs. 48 and 49). The prediction errors of the model corresponding to each test result are also presented.

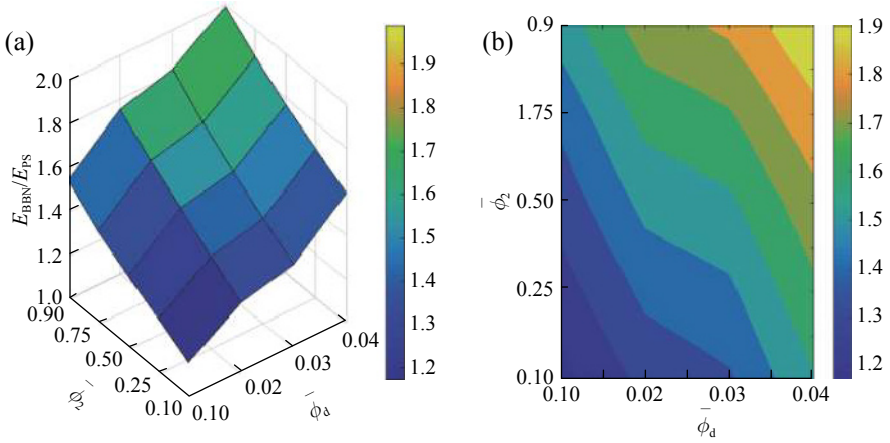

Fig. 12 (a) 3D plot of KAd result pattern for simultaneous variation of the contents of dispersed polymer phase and Janus nanoparticles in PS/PMMA/Janus BBN system, (b) contour plot. $\phi_{pi.}$, ϕ_{cr2} and $1-\phi_{cr1}$ are considered to be 0.5, 0.17 and 0.83 (vol%), respectively, and parameter y = 0.48% (Eqs. 48 and 49).

CONCLUSIONS

A specific type of blend based polymer nanocomposites (BBNs), as systems comprising polymer/polymer and dual polymer/particle interfaces, were analytically investigated. Synthesized Janus nanoparticles were used in order to ensure their migration toward polymer/polymer interface. It was assumed that the three-phase contact angle (β) of Janus nanoparticles at oil/water interface in Pickering emulsions was similar to that at polymer/polymer interface in BBN systems due to their specific surface chemistry after secondary surface modification stage (Fig. 1b). Accordingly, the modeling procedure was founded on two stages: first, modeling of polymer/polymer interface region *via* developing to the model proposed by Ji *et al*., and second, modeling of the whole BBN system *via* developing the model proposed by Wang *et al*. as a function of the variation of polymer blend morphology. In the first stage, all possible states of polymer/nanoparticle dual interphase around Janus nanoparticles in polymer/polymer interface region were considered and their corresponding geometrical structures were presented. In the second stage, the variation of blend morphology was investigated in four intervals plus phase inversion point and the corresponding geometrical structures were also presented. Consequently, the combination of stages one and two resulted in a comprehensive model which could cover all states of polymer/particle dual interphases as well as the morphology of blend base. Several different samples were prepared and subjected to tensile test in order to compare their measured tensile moduli with the predictions of the proposed model. The thicknesses of polymer/particles interphases were determined using NAS model and tensile results of PS/UAP1 and PMMA/UHP1 nanocomposites. It

https://doi.org/10.1007/s10118-019-2178-3

was revealed that the model is acceptably capable of predicting the tensile modulus of BBN systems comprising low contents of Janus nanoparticles (< 3 vol%), while at higher contents, the possible agglomeration of nanoparticles resulted in deviation between the actual and predicted values. Moreover, it was also proved that the model accuracy was not significantly affected by the morphology variation of the blend base. As a result, it can be claimed that the proposed model, as one of the first attempts to analytically investigate BBN systems comprising nanoparticles at polymer/polymer interface, is completely practical and can be definitely considered as a start point for further developments.

Electronic Supplementary Information

Electronic supplementary information (ESI) is available free of charge in the online version of this article at http://dx.doi.org/10.1007/s10118-019-2178-3.

REFERENCES

1 Fathi, A.; Lee, S.; Breen, A.; Shirazi, A. N.; Valtchev, P.; Dehghani, F. Enhancing the mechanical properties and physical stability of biomimetic polymer hydrogels for micro-patterning and tissue engineering applications. *Eur. Polym. J.* **2014**, *59*, 161−170.
2 Minaei-Zaim, M.; Ghasemi, I.; Karrabi, M.; Azizi, H. Effect of injection molding parameters on properties of cross-linked low-density polyethylene/ethylene vinyl acetate/organoclay nanocomposite foams. *Iran Polym. J.* **2012**, *21*, 537−546.
3 Shaw, M. T. in *Preparation of blends. in polymer blends and mixtures*. Walsh, D. J.; Higgins, J. S.; Maconnachie, A., Eds. Springer Netherlands, Dordrecht, **1985**, p57-67
4 Galloway, J. A.; Macosko, C. W. Comparison of methods for the detection of cocontinuity in poly(ethylene oxide)/polystyrene blends. *Polym. Eng. Sci.* **2004**, *44*, 714−727.
5 Zaikov, G. E.; Bazylyak, L. I.; Haghi, A. K. in *Functional polymer blends and nanocomposites: A practical engineering approach*. Apple Academic Press, **2014**
6 Miles, I. S.; Zurek, A. Preparation, structure, and properties of two-phase co-continuous polymer blends. *Polym. Eng. Sci.* **1988**, *28*, 796−805.
7 Pivsa-Art, W.; Chaiyasat, A.; Pivsa-Art, S.; Yamane, H.; Ohara, H. Preparation of polymer blends between poly(lactic acid) and poly(butylene adipate-*co*-terephthalate) and biodegradable polymers as compatibilizers. *Energy Procedia* **2013**, *34*, 549−554.
8 Khaparde, D. Preparation and prediction of physical properties of cellulose acetate and polyamide polymer blend. *Carbohydr. Polym.* **2017**, *173*, 338−343.
9 Lepcio, P.; Ondreas, F.; Zarybnicka, K.; Zboncak, M.; Caha, O.; Jancar, J. Bulk polymer nanocomposites with preparation protocol governed nanostructure: the origin and properties of aggregates and polymer bound clusters. *Soft Matter* **2018**, *14*, 2094−2103.
10 Ucankus, G.; Ercan, M.; Uzunoglu, D.; Culha, M., 1 - Methods for preparation of nanocomposites in environmental remediation A2 - Hussain, Chaudhery Mustansar. In *New polymer nanocomposites for environmental remediation*, Mishra, A. K., Ed. Elsevier, **2018**, pp 1-28
11 Mittal, V. in *Polymer nanotube nanocomposites: Synthesis, properties, and applications*. Wiley, **2010**
12 Koo, J. H. in *Fundamentals, properties, and applications of polymer nanocomposites*. Cambridge University Press, **2016**
13 Thomas, S.; Grohens, Y.; Jyotishkumar, P. in *Characterization of polymer blends: Miscibility, morphology and interfaces*. Wiley, **2014**
14 Isayev, A. I. in *Encyclopedia of polymer blends: volume 1: Fundamentals*. John Wiley & Sons, **2010**
15 Bai, L.; He, S.; Fruehwirth, J. W.; Stein, A.; Macosko, C. W.; Cheng, X. Localizing graphene at the interface of cocontinuous polymer blends: Morphology, rheology, and conductivity of cocontinuous conductive polymer composites. *J. Rheol.* **2017**, *61*, 575−587.
16 Landel, R. F.; Nielsen, L. E. in *Mechanical properties of polymers and composites*, Second Edition. Taylor & Francis, **1993**
17 Chiu, F. C.; Yen, H. Z.; Lee, C. E. Characterization of PP/HDPE blend-based nanocomposites using different maleated polyolefins as compatibilizers. *Polym. Test.* **2010**, *29*, 397−406.
18 Naffakh, M.; Diez-Pascual, A. M.; Marco, C. Polymer blend nanocomposites based on poly(L-lactic acid), polypropylene and WS_2 inorganic nanotubes. *RSC Adv.* **2016**, *6*, 40033−40044.
19 Baudouin, A. C.; Devaux, J.; Bailly, C. Localization of carbon nanotubes at the interface in blends of polyamide and ethylene-acrylate copolymer. *Polymer* **2010**, *51*, 1341−1354.
20 Sharifzadeh, E.; Salami-Kalajahi, M.; Hosseini, M. S.; Aghjeh, M. K. R. Synthesis of silica Janus nanoparticles by buoyancy effect-induced desymmetrization process and their placement at the PS/PMMA interface. *Colloid. Polym. Sci.* **2017**, *295*, 25−36.
21 Bryson, K. C.; Löbling, T. I.; Müller, A. H. E.; Russell, T. P.; Hayward, R. C. Using Janus nanoparticles to trap polymer blend morphologies during solvent-evaporation-induced demixing. *Macromolecules* **2015**, *48*, 4220−4227.
22 Paunov, V. N.; Cayre, O. J. Supraparticles and "Janus" particles fabricated by replication of particle monolayers at liquid surfaces using a gel trapping technique. *Adv. Mater.* **2004**, *16*, 788−791.
23 Lv, W.; Lee, K. J.; Li, J.; Park, T.-H.; Hwang, S.; Hart, A. J.; Zhang, F.; Lahann, J. Anisotropic Janus catalysts for spatially controlled chemical reactions. *Small* **2012**, *8*, 3116−3122.
24 Roh, K. H.; Martin, D. C.; Lahann, J. Biphasic Janus particles with nanoscale anisotropy. *Nat. Mater.* **2005**, *4*, 759.
25 Giermanska-Kahn, J.; Laine, V.; Arditty, S.; Schmitt, V.; Leal-Calderon, F. Particle-stabilized emulsions comprised of solid droplets. *Langmuir* **2005**, *21*, 4316−4323.
26 Fernandez-Rodriguez, M. A.; Rodriguez-Valverde, M. A.; Cabrerizo-Vilchez, M. A.; Hidalgo-Alvarez, R. Surface activity of Janus particles adsorbed at fluid-fluid interfaces: Theoretical and experimental aspects. *Adv. Colloid Interface Sci.* **2016**, *233*, 240−254.
27 Kango, S.; Kalia, S.; Celli, A.; Njuguna, J.; Habibi, Y.; Kumar, R. Surface modification of inorganic nanoparticles for development of organic–inorganic nanocomposites—A review. *Prog. Polym. Sci.* **2013**, *38*, 1232−1261.
28 Mahdavi, M.; Ahmad, M.; Haron, M.; Namvar, F.; Nadi, B.; Rahman, M.; Amin, J. Synthesis, surface modification and characterisation of biocompatible magnetic iron oxide nanoparticles for biomedical applications. *Molecules* **2013**, *18*, 7533−7548.
29 Taguet, A.; Cassagnau, P.; Lopez-Cuesta, J. M. Structuration, selective dispersion and compatibilizing effect of (nano)fillers in polymer blends. *Prog. Polym. Sci.* **2014**, *39*, 1526−1563.
30 Sharifzadeh, E.; Ghasemi, I.; Karrabi, M.; Azizi, H. A new approach in modeling of mechanical properties of binary phase polymeric blends. *Iran Polym. J.* **2014**, *23*, 525−530.
31 Sharifzadeh, E.; Ghasemi, I.; Karrabi, M.; Azizi, H. A new approach in modeling of mechanical properties of nanocompos-

ites: Effect of interface region and random orientation. *Iran Polym. J.* **2014**, *23*, 835−845.
32 Sharifzadeh, E.; Ghasemi, I.; Safajou-Jahankhanemlou, M. Modulus prediction of binary phase polymeric blends using symmetrical approximation systems as a new approach. *Iran Polym. J.* **2015**, *24*, 735−746.
33 Zare, Y. Modeling the strength and thickness of the interphase in polymer nanocomposite reinforced with spherical nanoparticles by a coupling methodology. *J. Colloid Interface Sci.* **2016**, *465*, 342−346.
34 Zare, Y. Modeling of tensile modulus in polymer/carbon nanotubes (CNT) nanocomposites. *Synth. Met.* **2015**, *202*, 68−72.
35 Zare, Y.; Rhee, K. Y.; Park, S. J. Modeling of tensile strength in polymer particulate nanocomposites based on material and interphase properties. *J. Appl. Polym. Sci.* **2017**, *134*, 44869.
36 Bao, W. S.; Meguid, S. A.; Zhu, Z. H.; Meguid, M. J. Modeling electrical conductivities of nanocomposites with aligned carbon nanotubes. *Nanotechnology* **2011**, *22*, 485704.
37 Zare, Y. Modeling approach for tensile strength of interphase layers in polymer nanocomposites. *J. Colloid Interface Sci.* **2016**, *471*, 89−93.
38 Sharifzadeh, E.; Ghasemi, I.; Qarebagh, A. N. Modeling of blend-based polymer nanocomposites using a knotted approximation of Young's modulus. *Iran Polym. J.* **2015**, *24*, 1039−1047.
39 Mortazavi, S.; Ghasemi, I.; Oromiehie, A. Prediction of tensile modulus of nanocomposites based on polymeric blends. *Iran Polym. J.* **2013**, *22*, 437−445.
40 Dong, B.; Huang, Z.; Chen, H.; Yan, L. T. Chain-stiffness-induced entropy effects mediate interfacial assembly of Janus nanoparticles in block copolymers: From interfacial nanostructures to optical responses. *Macromolecules* **2015**, *48*, 5385−5393.
41 Zhu, G.; Huang, Z.; Xu, Z.; Yan, L. T. Tailoring interfacial nanoparticle organization through entropy. *Acc. Chem. Res.* **2018**, *51*, 900−909.
42 Chen, P.; Yang, Y.; Dong, B.; Huang, Z.; Zhu, G.; Cao, Y.; Yan, L. T. Polymerization-induced interfacial self-assembly of Janus nanoparticles in block copolymers: Reaction-mediated entropy effects, diffusion dynamics, and tailorable micromechanical behaviors. *Macromolecules* **2017**, *50*, 2078−2091.
43 Ji, X. L.; Jing, J. K.; Jiang, W.; Jiang, B. Z. Tensile modulus of polymer nanocomposites. *Polym. Eng. Sci.* **2002**, *42*, 983−993.
44 Wang, J. F.; Carson, J. K.; North, M. F.; Cleland, D. J. A knotted and interconnected skeleton structural model for predicting Young's modulus of binary phase polymer blends. *Polym. Eng. Sci.* **2010**, *50*, 643−651.
45 Kolařík, J. Three-dimensional models for predicting the modulus and yield strength of polymer blends, foams, and particulate composites. *Polym. Compos.* **1997**, *18*, 433−441.
46 Sharifzadeh, E.; Salami-Kalajahi, M.; Hosseini, M. S.; Aghjeh, M. K. R. A temperature-controlled method to produce Janus nanoparticles using high internal interface systems: Experimental and theoretical approaches. *Colloid Surface A* **2016**, *506*, 56−62.
47 Sharifzadeh, E.; Salami-Kalajahi, M.; Salami Hosseini, M.; Razavi Aghjeh, M. K.; Najafi, S.; Jannati, R.; Hatef, Z. Defining the characteristics of spherical Janus particles by investigating the behavior of their corresponding particles at the oil/water interface in a Pickering emulsion. *J. Dispersion Sci. Technol.* **2017**, *38*, 985−991.
48 Mekhilef, N.; Verhoogt, H. Phase inversion and dual-phase continuity in polymer blends: Theoretical predictions and experimental results. *Polymer* **1996**, *37*, 4069−4077.

https://doi.org/10.1007/s10118-019-2178-3